analytical chemistry

Article

Cite This: *Anal. Chem.* 2019, 91, 12468−12475

pubs.acs.org/ac

Novel D-A-D-Type Supramolecular Aggregates with High Photoelectric Activity for Construction of Ultrasensitive Photoelectrochemical Biosensor

Han-Mei Deng, Ming-Hui Zhu, Liao-Jing Huang, Ya-Qin Chai, Xiao-Rui Liu, Ruo Yuan,* and Ya-Li Yuan*

Key Laboratory of Luminescent and Real-Time Analytical Chemistry (Southwest University), Ministry of Education, College of Chemistry and Chemical Engineering, Southwest University, Chongqing 400715, P.R. China

Supporting Information

ABSTRACT: In this work, hydrazine-functionalized perylene diimide derivative supramolecular (HPDS), a novel self-enhanced donor−acceptor-donor (D-A-D) type aggregates with excellent photoelectric activity, was synthesized by a facile one-pot green route and further applied in construction of coreactant-free photoelectrochemical (PEC) biosensor for ultrasensitive DNA assay. Impressively, the HPDS formed by D-A-D units not only possessed effectively shorted electron-transfer path between donor and acceptor, but also presented a desiring aggregate state via the $\pi-\pi$ stacking of perylene core and hydrogen bonding of the terminal moiety, thereby acquiring a high density electron flow for generating the extremely high PEC signal. Experimental data showed that the well film-formed HPDS aggregate could produce an exciting photocurrent intensity about 6-fold stronger than that of precursor perylene dianhydride with donor N_2H_4 in detection buffer and even 12-fold than that of perylene dianhydride only. In this respect, the resultant HPDS aggregate as a novel self-enhanced PEC signal tag was adopted to fabricate the coreactant-free PEC biosensor with the help of target dual-recycling-induced bipedal DNA walker cascade amplification strategy for ultrasensitive DNA (a fragment of TP53 gene) assay. The proposed biosensor showed a high sensitivity with a low detection limit down to femtomole level, providing a new avenue for sensitive bioanalysis and clinical diagnosis.

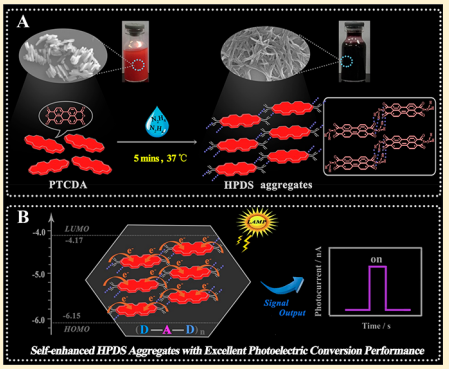

Photoactive material, an integral part in photoelectrochemical (PEC) bioanalysis system for signal generation, has aroused great attention in recent years because of the compact relationship with detection sensitivity.[1−5] Commonly, the electron donors/acceptors (D/A) existed in electrolyte solution[6−8] or in situ generated via biocatalytic reactions[9−12] were adopted for improving the PEC signal of photoactive material, which thus inevitably suffered from defects of tedious operation, batch-to-batch variation, and low photon-to-electricity conversion efficiency on account of the separation from photoactive materials. Comparatively, merging electron D/A into photoactive material within a molecule to form the newly self-enhanced materials (denoted as D-A-type) might effectively resolve these issues.[13−15] However, the synthesis of these self-enhanced photoactive material was complicated and rigorous. Most importantly, self-enhanced photoactive material in a monodispersed state limited the further improvement of the PEC signal. In this respect, we synthesized highly photoactive self-enhanced donor−acceptor−donor (D-A-D) type aggregates, hydrazine-functionalized perylene diimide derivative supramolecular (HPDS), by a facile one-pot green route. The electron-donating hydrazine moiety at both sides of the electron-deficient perylene core could effectively shorten the inter electron-transfer path and reduce energy loss. More importantly, the formed D-A-D units could gather together to generate aggregated HPDS nanobelts via $\pi-\pi$ stacking of perylene core and hydrogen bonding of hydrazine moiety, by which a high density electron flow could thus be obtained for acquiring extremely high PEC signal, providing a novel self-enhanced PEC signal tag for constructing sensitive coreactant-free PEC biomolecule assay systems without extra introduce of sensitizer or electron donors/acceptors (D/A) reagent into the testing electrolyte.

DNA walker machine is one of the artificial molecular machines constructed by smart synthetic DNA, which can carry out autonomously and directionally quasi-mechanical motion in response to the external stimuli such as ions and enzymes,[16−18] providing the broad application prospect in construction of sensitive and specific biosensors.[19−21] Hence, we proposed a novel target dual-recycling-induced bipedal DNA walker cascade amplification strategy in the help of exonuclease III (Exo III) to convert a small amount of target DNA into substantial output DNAs for further improving the

Received: July 11, 2019
Accepted: September 2, 2019
Published: September 2, 2019

DOI: 10.1021/acs.analchem.9b03151
Anal. Chem. 2019, 91, 12468−12475

Scheme 1. Schematic Diagrams of Sensitive PEC Biosensor for the DNA Assay: (A) Preparation Process of HPDS Aggregates, (B) Construction of the Proposed Biosensor, (C) Photoelectric Conversion Mechanism of HPDS Aggregates, and (D) the Target Dual-Recycling-Induced Bipedal DNA Walker Cascade Amplification with the Assistance of Exo III

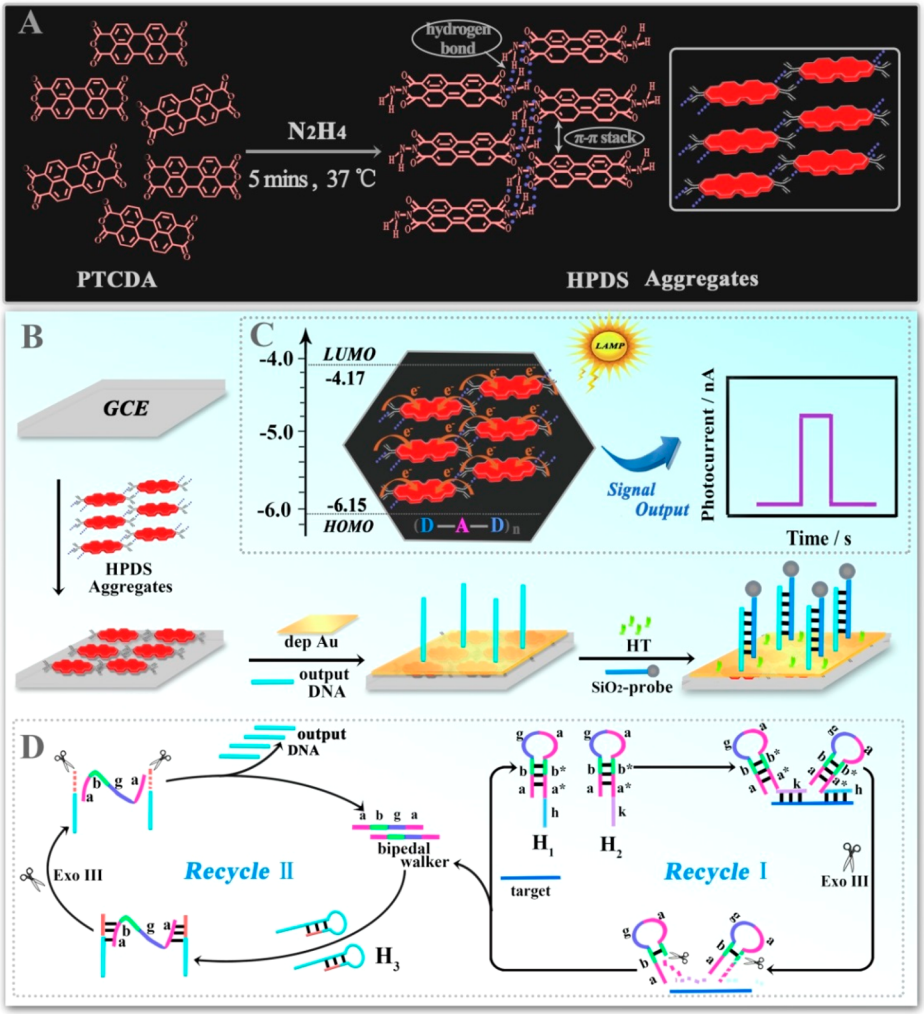

sensitivity of biosensors. Compared with traditional strategies using target single-recycling-induced single-pedal DNA walker cascade amplification,[22−24] the proposed strategy adopted the target DNA with two different binding domains to simultaneously interact with two kinds of hairpin DNA for triggering target double-recycle and thus releasing terminal symmetrical bipedal DNA walkers (contains two identical binding domains) for continuously opening of dual hairpin DNA, thereby generating substantial output DNAs with prominent improvement of amplification capability.

Herein, by utilizing the well film-formed HPDS aggregates with excellent photoactivity as sensing platform, we proposed an ultrasensitive coreactant-free PEC biosensor on the basis of the target dual-recycling-induced bipedal DNA walker cascade amplification. As depicted in Scheme 1, HPDS aggregates were directly anchored on the electrode, thus endowing the generation of extremely high initial PEC signal. Meanwhile, the target DNA with two binding domains was synchronously hybridized with the distinct toeholds of two types of hairpins (H_1 and H_2) to form a triplex junction structure, in which each hairpin was subsequently cleavaged by Exo III for release of target DNA for recycle (cycle I) and production of double terminal symmetrical bipedal DNA walkers for triggering next newly recycle (cycle II). Surprisingly, the bipedal DNA walkers with two identical binding domains could trigger Exo III-assisted recycling amplification, thereby generating numerous output DNAs, which could be immobilized on the electrode for assembling inert SiO_2 nanoparticles to quench photocurrent signal for sensitive target assay. This strategy not only synthesized a novel self-enhanced PEC signal tag but also proposed an effective cascade amplification strategy, providing a new avenue at sensitive assay for the application in bioanalysis and clinical diagnosis.

EXPERIMENTAL SECTION

One-Step, Green, and High-Yielding Synthesis of HPDS Aggregates. First, 0.02 g PTCDA was first added into 2 mL deionized water with vigorously stirring. Afterward, 40 mL hydrazine monohydrate ($N_2H_4{\cdot}H_2O$) was quickly added to the above solution, accompanying with the color changes of solution from bright red to dark purple. To verify whether the reaction proceed thoroughly, strong alkal (NaOH) was added into the above suspension solution. Interestingly, the bright yellow solution with strong fluorescent belonged to hydrolysate (PTC^-) of PTCDA did not monitored, which demonstrated that PTCDA as synthetic precursor was

DOI: 10.1021/acs.analchem.9b03151
Anal. Chem. 2019, 91, 12468−12475

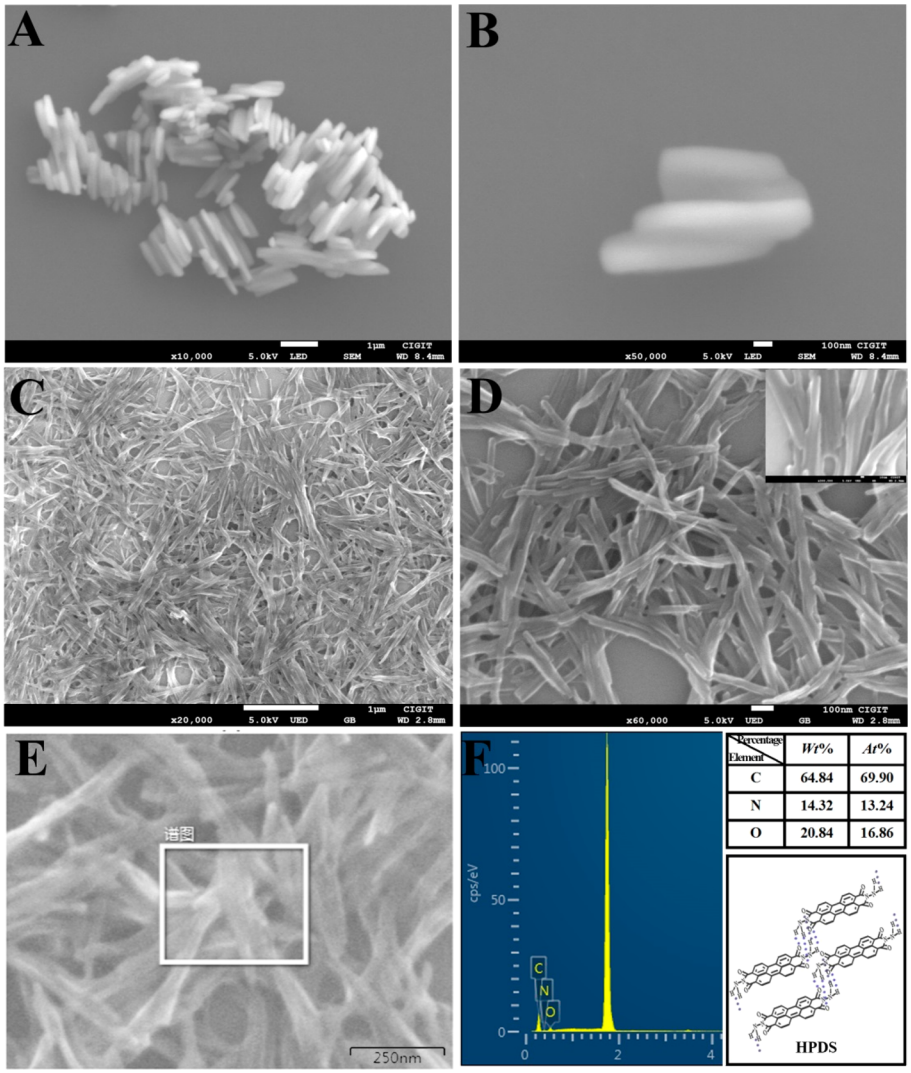

Figure 1. SEM images of (A) PTCDA nanorods, (B) single enlarged PTCDA nanorods, (C) synthesized HPDS aggregate nanomaterials, and (D) the magnified HPDS aggregate nanobelts (insert: enlarged SEM image on the surface of nanobelts). (E) The sampling region of EDS analysis of HPDS aggregates and (F) the corresponding EDS analysis spectrogram.

completely converted into HPDS within several minutes via a one-pot, green, and high-yielding procedure. After being centrifuged and washed with deionized water, dark red precipitate HPDS aggregates were collected through a simple and effective purification and restored in deionized water for further use.

Fabrication of HPDS-Based Biosensor for the TP53 Gene Assays. In the absence of any coreaction reagent (electronic donor or receptor) at electrolyte solution, self-enhanced HPDS aggregates held an outstanding PEC response, thus HPDS aggregates as excellent photoactive material was applied to construct PEC biosensor for ultrasensitive assay. Here, based on D-A-D-typed HPDS aggregates, a sensitive PEC biosensor was proposed for the detection of DNA with the assistance of Exo III-triggered double bipedal DNA walker cascade amplification. First, 50 μL H_1 (2 μM), 50 μL H_2 (2 μM) and 10 μL various concentrations of TP53 gene were mixed together and incubated 2 h at 37 °C. Simultaneously, H_3 was treated by reduction buffer containing 10 mM Tris(2-carboxyethyl)phosphine (TCEP) for avoiding the formation of S−S bond. After that, 50 μL 4 μM H_3 and 80 U Exo III were added and then incubated 30 min at 37 °C to trigger double bipedal DNA walker cascade amplification, which subsequently produced massive output DNA for the further use. Meanwhile, 15 μL prepared HPDS aggregates were dropped on the mirror-like cleaned glassy carbon electrode (GCE) with the drying treatment. Afterward, then AuNPs was deposited on the surface. And then 10 μL output DNA from the Exo III-triggered double bipedal DNA walker cascade amplification was incubated at modified electrode for 12 h at 4 °C. After that, 1 mM 5 μL HT was added to block remaining binding sites of AuNPs. 100 μL SiO_2−NH_2 NPs prepared according to the previous report[25] and dialdehyde solution were added into 10 μL 100 μM amino-labeled capture DNA for obtaining SiO_2-labeled DNA linkers through 2 h cross-linking reaction at 37 °C. Finally, 5 μL SiO_2-labeled DNA linkers were introduced to immobilize on GCE through hybridization with output DNA.

RESULTS AND DISCUSSION

Morphology and Component Characterization of the Nanomaterials. SEM was employed to characterize the surface morphologies of nanomaterials. PTCDA as raw material for the synthesis of HPDS exhibited a short and

DOI: 10.1021/acs.analchem.9b03151
Anal. Chem. 2019, 91, 12468−12475

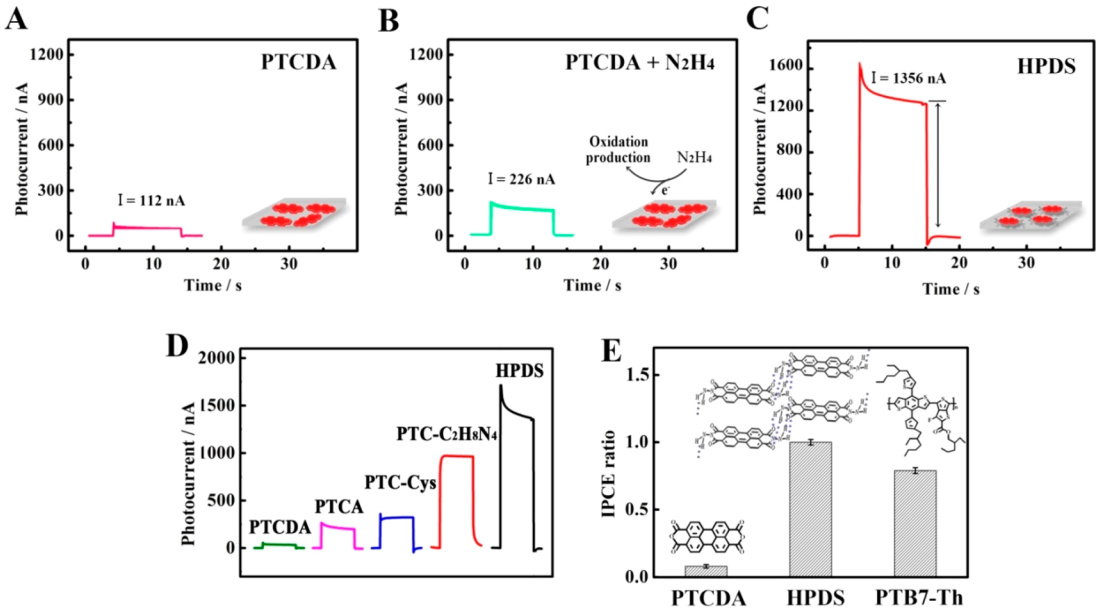

Figure 2. Photocurrent responses of (A) PTCDA at PBS (pH 7.4) electrolyte solution, (B) PTCDA at PBS (pH 7.4) electrolyte solution including N_2H_4, and (C) HPDS at PBS (pH 7.4) electrolyte solution under the same amount. (D) The photocurrent intensity of diverse perylene derivatives materials including PTCDA, PTCA, PTC-Cys, PTC-$C_2H_8N_2$, and HPDS. (E) The IPCE ratio of PTCDA and PTB7-Th relative to HPDS.

thick rod-like structure (Figure 1A), and the enlarged view of single stick morphology is shown in Figure 1B. In comparison, HPDS aggregate with nanobelts structure was more slender and longer than PTCDA (Figure 1C), which mainly attributed to the synergetic effect of intermolecular $\pi-\pi$ stacking and H-bonding at the both sides. Additionally, the locally magnified vision and further enlarged partial image of HPDS aggregate were respectively displayed in Figure 1D and the corresponding inset picture. Furthermore, the component of HPDS aggregate was investigated by SEM-EDS analysis. The sampling region of EDS analysis was shown at Figure 1E, and the measured elements peaks demonstrated that the atomic percentages of C, N, and O was 69.9%, 13.24%, and 16.86% (Figure 1F), which were in good agreement with expected elemental component of HPDS aggregates.

Characterization of the Photoelectric Properties for Synthetic HPDS Aggregates. To explore the photoelectric performance of self-enhanced HPDS aggregates, the same amount of PTCDA and HPDS aggregates were respectively film-formed at working electrode to monitor the photocurrent response in PBS (pH 7.4) electrolyte solution. As shown in Figure 2A, PTCDA as the synthetic precursors of HPDS aggregates exhibited a tiny signal (112 nA). While extra adding N_2H_4 as electron donor reagent of PTCDA into electrolyte solution, a slightly enhanced signal (226 nA) appeared (Figure 2B), indicating that N_2H_4 at electrolyte solution could be served as electron donor to trap photogenerated hole of photoactive material for facilitating generation of photocurrent. Notably, as shown in Figure 2C, HPDS aggregates held a significant photocurrent response (1356 nA) about 12-fold stronger than that of PTCDA alone and even 6-times as high as PTCDA detected at N_2H_4 solution, indicating that, at HPDS aggregates, terminal hydrazine moiety at both sides as electron-donating group was corporated with electron-deficient perylene core to generate the self-enhanced donor−acceptor−donor (D-A-D) unit within a molecule, thus effectively shorting the electron-transfer path between donor and acceptor. Besides that, the formed D-A-D units could gather together to generate the aggregated supramolecular (HPDS) via the $\pi-\pi$ stacking of perylene core and hydrogen bonding of terminal moiety, by which an accelerated carrier mobility with high density electron flow could thus be obtained for acquiring dramatically improved PEC signal. Moreover, the photoelectric performance of self-enhanced HPDS aggregates was investigated in comparison with photocurrent intensity of diverse perylene derivatives materials including PTCDA, PTCA,[26] ethylenediamine-functionalized perylene (PTC-$C_2H_8N_2$),[27] and cysteine-functionalized perylene (PTC-Cys).[28] As shown in Figure 2D, PTCA, PTC-Cys, and PTC-$C_2H_8N_2$ all presented a better photoelectric performance than that of PTCDA as synthetic precursor. By comparison, HPDS aggregates held a significant photocurrent response with a stronger signal than the others. Furthermore, to further verify the outstanding photoelectric conversion capability of HPDS aggregates, PTCDA and D-A-typed poly{4,8-bis[5-(2-ethylhexyl)thiophen-2-yl]benzo[1,2-b:4,5-b] dithiophene-2,6-diyl-alt-3-fluoro-2-[(2-ethylhexyl)carbonyl]thieno[3,4-*b*]-thiophene-4,6-diyl} (PTB7-Th) as traditionally self-enhanced photoactive material in PEC biosensors were employed to compare the incident photon-to-electron conversion efficiency (IPCE) of synthetic HPDS aggregates, IPCE[29] was defined as the ratio of photocurrent intensity to incident photon in terms of monochromatic source:

$$\begin{aligned}\mathrm{IPCE} &= \mathrm{EQE} \\ &= [|J_{ph}|(\mathrm{mA/cm^2}) \times 1240(\mathrm{v^*nm})]/[P_{mono}(\mathrm{mw/cm^2}) \\ &\quad \times \lambda(\mathrm{nm})]\end{aligned}$$

where J_{ph}, P_{mono}, and λ are the photocurrent intensity, illumination power density, and monochromatic wavelength, respectively. The calculated IPCE value of PTB7-Th was about 0.79-fold lower than that of HPDS, and the IPCE value of raw materials was as low as 0.08-fold than that of HPDS (Figure 2E), which indicated that D-A-D typed HPDS aggregates had an excellent photon-to-electron conversion efficiency.

DOI: 10.1021/acs.analchem.9b03151
Anal. Chem. 2019, 91, 12468−12475

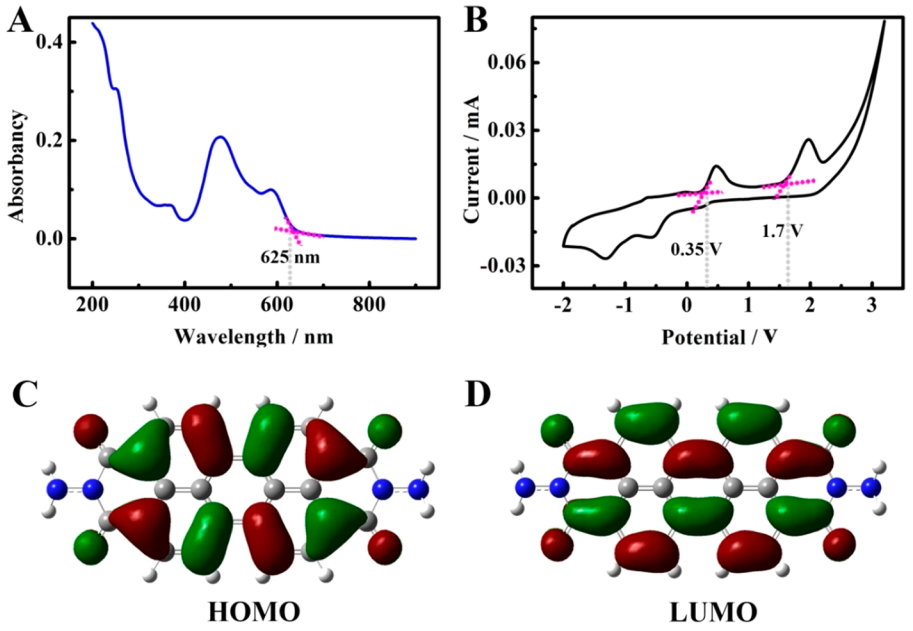

Figure 3. (A) UV−vis absorption spectrum and (B) CV curve of HPDS aggregates. The frontier molecular orbital densities of (C) HOMO and (D) LUMO.

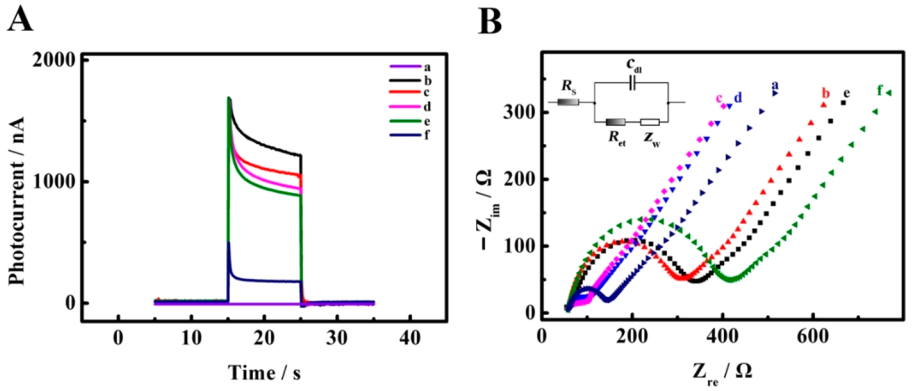

Figure 4. (A) PEC and (B) EIS responses of (a) bare GCE, (b) HPDS/GCE, (c) depAu/HPDS/GCE, (d) output DNA/depAu/HPDS/GCE, (e) HT/output DNA/depAu/HPDS/GCE, and (f) SiO_2-labeled DNA/HT/output DNA/depAu/HPDS/GCE.

Energy Gap (E_g) and Energy Levels Characterization of HPDS Aggregates. UV−vis absorption spectrum and CV measurements were performed to estimate the energy gap (E_g) of HPDS and the involved energy levels of the LUMO and HOMO. Typical characteristic absorption peaks from the visible region to near-infrared zone were recorded at the UV−vis absorptionspectrum (Figure 3A), the cutoff wavelength at 625 nm was then applied to estimate the value of E_g, which was calculated to be 1.98 eV according to the eq 1, where the Eg_{HPDS} represented the energy gap (E_g) of HPDS aggregates nanomaterial.[30]

$$E_{g_{HPDS}} = 1240/\lambda_{cutoff} \quad (1)$$

Moreover, the HOMO and LOMO levels of the HPDS aggregates were further investigated through CV measurement at anhydrous CH_3CN solution containing 1 M Bu_4NPF_6 (as the supporting electrolyte) and Fc (as an external standard). As shown in Figure 3B, notable oxidation potential of Fc and HPDS aggregates ($E_{OX(Fc)}$ and $E_{OX(HPDS)}$ represented the oxidation potentials of the Fc and HPDS aggregates, respectively) were respectively located at 0.35 and 1.7 V. According to these available oxidation potentials, $HOMO_{HPDS}$(refers to the HOMO of HPDS aggregates nanomaterial) was counted to be −6.15 eV by eq 2. Subsequently, computing value of $LUMO_{HPDS}$(refers to the LUMO of HPDS aggregates nanomaterial) was −4.17 eV with the utilization of eq 3.

$$HOMO_{HPDS} = -(4.8\ eV - E_{OX(Fc)} + E_{OX(HPDS)}) \quad (2)$$

$$LUMO_{HPDS} = HUMO_{HPDS} + E_{g_{HPDS}} \quad (3)$$

Furthermore, frontier molecular orbitals of HPDS were displayed at Figure 3C,D, and the density functional theory (DFT) calculations at the HSEh1PBE/6-311G (d,p) levels were carried out to estimate the theory values of HOMO and LUMO. Theoretical calculation values were −6.19 and −4.07 eV, respectively, illustrating that the experimental results were agreed with the theoretical ones.

PEC and EIS Characterizations of the HPDS-Based Biosensor. PEC and EIS characterization were carried out to investigate the step-by-step assembly procedures of the fabricated electrode. Corresponding PEC characterization

DOI: 10.1021/acs.analchem.9b03151
Anal. Chem. 2019, 91, 12468−12475

was shown in Figure 4A, after coating HPDS aggregates photoactive materials on the bare electrode, a significant increase of the photocurrent response (curve b) was obtained compared with that of the bare GCE (curve a), which was attributed to the excellent photoelectric activity of the self-enhanced HPDS aggregates photoactive materials. However, when AuNPs were deposited on the above electrode, photocurrent response decreased slightly due to the large specific surface area of depAu (deposition of AuNPs) for the light absorption of HPDS aggregates photoactive material (curve c). Subsequently, incubation of the output DNA from the cascade amplification caused a subtle decrease on account of the poor charge transfer of DNA skeleton (curve d). And then, photocurrent response further decreased with the assembly of HT on electrode (curve e). Followed by the modification of the SiO_2-labeled DNA, photocurrent response was decreased greatly, which was mainly ascribed to the inhibition of electrons transfer and increase of the steric hindrance (curve f).

Furthermore, EIS characterization was investigated to further confirm the stepwise fabrication process of the biosensor, and the result was shown in Figure 4B. The charge-transfer resistance (R_{et}) curve of the bare GCE displayed a small semicircle and long tail (curve a). After dropping HPDS on the bare GCE, an obvious increase of the R_{et} response was observed (curve b). When AuNPs were coated on HPDS materials, R_{et} response decreased owing to the good conductivity of AuNPs (curve c). Afterward, the R_{et} response increased sequentially for the incubation of output DNA (curve d) and HT (curve e), which was on account of the electrostatic repulsion of the nucleotide sequences and blocking electron transfer of nonconductive HT. Finally, a dramatically increased R_{et} response was recorded (curve f) with the modification of SiO_2-labeled probes, which was primarily caused by the poor conductivity of SiO_2.

PAGE Characterization of DNA Walker Cascade Amplification Reaction. The PAGE analysis was investigated to verify the successful implementation of the Exo III-assisted bipedal DNA walker cascade amplification process. As shown in Figure 5, single band of lane 1−4 presented the PAGE results for the single-stranded DNA of H_1, H_2, H_3 and target DNA, respectively. The junction structures from the hybridization of H_1, H_2, and target DNA were observed at lane 5 with a slower migration (migrated direction from top to bottom) owing to a longer oligonucleotide than these single-stranded DNA. After simultaneous addition of H_3 and the Exo III for triggering cascade amplification cycle, the PAGE results showed three distinct bands (lane 6): one band exhibited a similar migration with the band of lane 4 on account of releasing target DNA from cascade amplification reaction, the second band moved faster than H_3, which implied that output DNA with shorter bases was newly emerged, and the remaining bands migrated more slower than junction structure, thereby indicating the appearance of bipedal walker DNA. As expected, above result demonstrated that target-initiated cascade amplification occurred at the assistance of Exo III. Whereas, in the absence of Exo III, two bands respectively belonged to junction structures and H_3 were distinct displayed at lane 7 from top to bottom, implied that cascade amplification reaction did not occurred without the drive of Exo III.

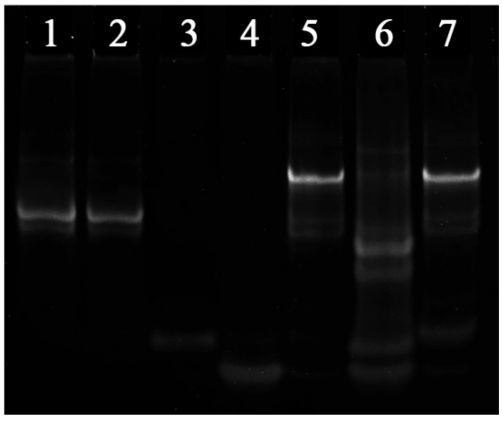

Figure 5. PAGE analysis: lane 1, H_1; lane 2, H_2; lane 3, H_3; lane 4, target DNA; lane 5, the junction structure; lane 6, the junction structure + Exo III + H_3; and lane 7, the junction structure+H_3.

Performance of the HPDS-Based Biosensor. In order to monitor the performance of proposed PEC biosensor, various concentrations of target was incubated at the optimal conditions. As shown in Figure 6A, the photocurrent signals were correspondingly reduced as increase of the target in the range of 2 fM to 50 nM and presented a desirable linear relationship with the logarithm of target concentration. The corresponding linear equation was demonstrated as $I = -1.060 \lg c + 3.48$ at Figure 6B with the correlation coefficient of 0.9968 (I indicated the photocurrent intensity, and lg$c$ was the logarithm of target concentration). The calculated limit of detection (LOD) was 0.64 fM (3 S_b/N), and the added error bar implied the detection standard deviation (n = 8). Furthermore, the assay performance comparison of the biosensor based on DNA walker-triggered amplification strategy for the detection of DNA was listed at table S2, which manifested the proposed biosensor had higher sensitivity in virtue of self-enhanced D-A-D-typed HPDS nanomaterial.

Selectivity, Stability, and Preliminary Application of the HPDS-Based Biosensor. To investigate the selectivity of fabricated biosensor, blank group and the 10-fold interference substances including miRNA-21, miRNA-155, miRNA-141, thrombin, and P53 gene were employed to estimate specificity, respectively. In the presence of various miRNA, thrombin and P53 gene (10 nM), photocurrent signals exhibited no notable change in comparison with that of blank group and the added error bar implied the detection standard deviation (n = 8), whereas minute quantities of target (1 nM) result in a singinificatly decreased PEC signal (Figure 6C), indicating that the proposed PEC biosensor possessed an excellent selectivity toward target DNA. Additionally, a continually periodical "off-on−off" light of 10 cycles was applied to explore the stability of proposed biosensor, stable signals was observed at Figure 6D with the relative standard deviation (RSD) of 1.27%. Furthermore, applicability of the HPDS-based biosensors was estimated by standard addition method. Briefly, diverse concentrations (10 fM, 1 pM, 10 pM, and 1 nM) of target DNA (TP53 gene related DNA fragment) were respectively blended into 50-fold diluted healthy serum, followed by measurement through fabricated biosensor. Results were presented as tabulated in table S3, and the recoveries ranged from 92.6% to 102.4% were verified that proposed biosensor was potential application in real sample assay.

DOI: 10.1021/acs.analchem.9b03151
Anal. Chem. 2019, 91, 12468−12475

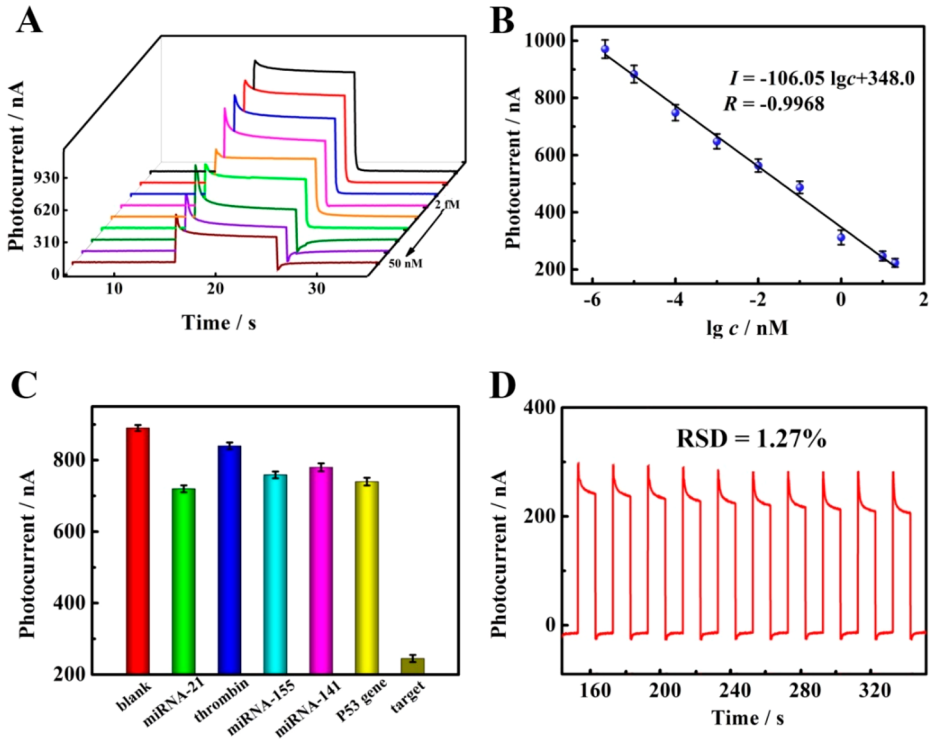

Figure 6. (A) Photocurrent responses of PEC biosensor toward detecting various concentrations of target: 2 fM, 10 fM, 100 fM, 1 pM, 10 pM, 100 pM, 1 nM, 10 nM, and 50 nM (from back to front). (B) The corresponding linear equation for the detection of target. (C) Photocurrent signal of the fabricated biosensor toward blank control group and diverse substances: 10 nM miRNA-21, 10 nM miRNA-155, 10 nM miRNA-141, 10 nM thrombin, 10 nM P53 gene and 1 nM target. (D) The stability of biosensor under the periodical "off-on−off" light for 10 cycles.

CONCLUSION

To summarize, we synthesized a self-enhanced D-A-D-type perylene diimide derivative by coupling electron-rich hydrazine with electron-deficient perylene core at intramolecular, followed by self-assembled, accumulation for forming HPDS aggregates via the $\pi-\pi$ stacking of perylene core and hydrogen bonding of terminal moiety. Significantly, with the integration of target dual-recycling-induced bipedal DNA walker cascade amplification, we proposed a coreactant-free PEC biosensor for ultrasensitive DNA (a fragment of TP53 gene) assay based on the well film-formed HPDS aggregate as platform. The proposed biosensor showed a high sensitivity, providing a new avenue for sensitive bioanalysis and clinical diagnosis.

ASSOCIATED CONTENT

Supporting Information

The Supporting Information is available free of charge on the ACS Publications website at DOI: 10.1021/acs.analchem.9b03151.

Reagents, materials, apparatus, structure characteristics of HPDS aggregate, simulation of the arrangement structure of HPDS aggregate, and optimization of the reaction conditions (PDF)

AUTHOR INFORMATION

Corresponding Authors

*Tel.: +86-23-68252277. Fax: +86-23-68253172. E-mail: yuanruo@swu.edu.cn.

*E-mail: y198688@swu.edu.cn.

ORCID

Ya-Qin Chai: 0000-0003-4392-9592

Ruo Yuan: 0000-0003-3664-6236

Notes

The authors declare no competing financial interest.

ACKNOWLEDGMENTS

This work was supported by the Chongqing Research Program of Basic Research and Frontier Technology (cstc2018jcyjA0797), the Fundamental Research Funds for the Central Universities (XDJK2019B022, SWU117045, and XDJK2018C041), and the National Natural Science Foundation (NNSF) of China (51473136 and 21575116).

REFERENCES

(1) Jian, J.; Xu, Y. X.; Yang, X. K.; Liu, W.; Fu, M. S.; Yu, H. W.; Xu, F.; Feng, F.; Jia, L. C.; Friedrich, D.; Krol, R. D.; Wang, H. Q. *Nat. Commun.* **2019**, *10* (1), 2609.

(2) Windle, C. D.; Kumagai, H.; Higashi, M.; Brisse, R.; Bold, S.; Jousselme, B.; Chavarot-Kerlidou, M.; Maeda, K.; Abe, R.; Ishitani, O.; Artero, V. *J. Am. Chem. Soc.* **2019**, *141*, 9593−9602.

(3) Li, R. R.; Tu, W. W.; Wang, H. S.; Dai, Z. H. *Anal. Chem.* **2018**, *90*, 9403−9409.

(4) Han, F. J.; Song, Z. Q.; Nawaz, M. H.; Dai, M. J.; Han, D. F.; Han, L. P.; Fan, Y. Y.; Xu, J. N.; Han, D. X.; Niu, L. *Anal. Chem.* **2019**, *91*, 10657−10662.

(5) Wang, L. N.; Ma, W. G.; Gan, S. Y.; Han, D. X.; Zhang, Q. X.; Niu, L. *Anal. Chem.* **2014**, *86*, 10171−10178.

(6) Zhang, N.; Ruan, Y. F.; Zhang, L. B.; Zhao, W. W.; Xu, J. J.; Chen, H. Y. *Anal. Chem.* **2018**, *90*, 2341−2347.

(7) Yang, R. Y.; Zou, K.; Li, Y. M.; Meng, L. X.; Zhang, X. H.; Chen, J. H. *Anal. Chem.* **2018**, *90*, 9480−9486.

(8) Hou, T.; Xu, N. N.; Wang, W. X.; Ge, L.; Li, F. *Anal. Chem.* **2018**, *90*, 9591−9597.

(9) Cui, L.; Hu, J.; Wang, M.; Diao, X. K.; Li, C. C.; Zhang, C. Y. *Anal. Chem.* **2018**, *90*, 11478−11485.

DOI: 10.1021/acs.analchem.9b03151
Anal. Chem. 2019, 91, 12468−12475

(10) Zhao, W. W.; Ma, Z. Y.; Xu, J. J.; Chen, H. Y. *Anal. Chem.* **2013**, *85*, 8503−8506.
(11) Ma, Z. Y.; Xu, F.; Qin, Y.; Zhao, W. W.; Xu, J. J.; Chen, H. Y. *Anal. Chem.* **2016**, *88*, 4183−4187.
(12) Shen, Q. M.; Han, L.; Fan, G. C.; Zhang, J. R.; Jiang, L. P.; Zhu, J. J. *Anal. Chem.* **2015**, *87*, 4949−4956.
(13) Zheng, Y. N.; Liang, W. B.; Xiong, C. Y.; Yuan, Y. L.; Chai, Y. Q.; Yuan, R. *Anal. Chem.* **2016**, *88*, 8698−8705.
(14) Xia, L. Y.; Zheng, Y. N.; Liang, W. B.; Li, M. J.; Hu, T.; Yuan, R.; Chai, Y. Q. *Chem. - Eur. J.* **2019**, *25*, 4087−4092.
(15) Hu, T.; Zheng, Y. N.; Li, M. J.; Liang, W. B.; Chai, Y. Q.; Yuan, R. *Anal. Chem.* **2018**, *90*, 6096−6101.
(16) Shin, J. H.; Pierce, N. A. *J. Am. Chem. Soc.* **2004**, *126*, 10834−10835.
(17) He, M. Q.; Wang, K.; Wang, W. J.; Yu, Y. L.; Wang, J. H. *Anal. Chem.* **2017**, *89*, 9292−9298.
(18) Ge, L.; Wang, W. X.; Sun, X. M.; Hou, T.; Li, F. *Anal. Chem.* **2016**, *88*, 2212−2219.
(19) Li, W.; Wang, L.; Jiang, W. *Chem. Commun.* **2017**, *53*, 5527−5530.
(20) Jung, C.; Allen, P. B.; Ellington, A. D. *ACS Nano* **2017**, *11*, 8047−8054.
(21) Phillips, E. A.; Moehling, T. J.; Bhadra, S.; Ellington, A. D.; Linnes, J. C. *Anal. Chem.* **2018**, *90*, 6580−6586.
(22) Li, W.; Wang, L.; Jiang, W. *Chem. Commun.* **2017**, *53*, 5527−5530.
(23) Xu, Z. Q.; Liao, L. L.; Chai, Y. Q.; Wang, H. J.; Yuan, R. *Anal. Chem.* **2017**, *89*, 8282−8287.
(24) Yan, T. T.; Zhu, L. Y.; Ju, H. X.; Lei, J. P. *Anal. Chem.* **2018**, *90*, 14493−14499.
(25) Wang, H. H.; Li, M. J.; Zheng, Y. N.; Hu, T.; Chai, Y. Q.; Yuan, R. *Biosens. Bioelectron.* **2018**, *120*, 71−76.
(26) Wang, S. Y.; Chen, C. S.; Yu, Z. H.; He, Y. L.; Chen, X. Y.; Wan, Q.; Shi, Y.; Zhang, D. W.; Zhou, H.; Wang, X. R.; Zhou, P. *Adv. Mater.* **2019**, *31*, 1806227.
(27) Lei, Y. M.; Huang, W. X.; Zhao, M.; Chai, Y. Q.; Yuan, R.; Zhuo, Y. *Anal. Chem.* **2015**, *87*, 7787−7794.
(28) Zhang, W.; Chai, Y. Q.; Yuan, R.; Han, J.; Chen, S. H. *Sens. Actuators, B* **2013**, *183*, 157−162.
(29) Choudhary, S.; Upadhyay, S.; Kumar, P.; Singh, N.; Satsangi, V. R.; Shrivastav, R.; Dass, S. *Int. J. Hydrogen Energy* **2012**, *37*, 18713−18730.
(30) Zhang, N.; Ruan, Y. F.; Zhang, L. B.; Zhao, W. W.; Xu, J. J.; Chen, H. Y. *Anal. Chem.* **2018**, *90*, 2341−2347.

DOI: 10.1021/acs.analchem.9b03151
Anal. Chem. 2019, 91, 12468−12475